Journal of Sound and Vibration 329 (2010) 3218–3232

Contents lists available at ScienceDirect

Journal of Sound and Vibration

journal homepage: www.elsevier.com/locate/jsvi

An adhesive bond state classification method for a composite skin-to-spar joint using chaotic insonification

Timothy R. Fasel, Michael D. Todd *

University of California, San Diego, 9500 Gilman Drive, La Jolla, CA 92093-0085, United States

ARTICLE INFO

Article history:
Received 12 July 2009
Received in revised form
28 January 2010
Accepted 3 February 2010
Handling Editor: A.V. Metrikine
Available online 20 February 2010

ABSTRACT

The combination of chaotically amplitude-modulated ultrasonic waves and time series prediction algorithms has shown the ability to locate and classify various bond state damage conditions of a composite bonded joint. This study examines the ability of a new two-part supervised learning classification scheme not only to classify disbond size but also to classify whether a bond for which there is no baseline data is undamaged or has some form of disbond. This classification is performed using data from a similarly configured composite bond for which baseline data are available. The test structures are analogous to a wing skin-to-spar bonded joint. An active excitation signal is imparted to the structure through a macro fiber composite (MFC) patch on one side of the bonded joint and sensed using an equivalent MFC patch on the opposite side of the joint. There is an MFC actuator/sensor pair for each bond condition to be identified. The classification approach compares features derived from an autoregressive (AR) model coefficient vector cross-assurance criterion.

1. Introduction

The emergence of bonded composite joints as a staple in many structural systems, particularly in the aerospace industry where composites are increasingly being deployed due to weight concerns, has introduced a need for *in situ* damage identification methods that are less intrusive and costly than the off-line techniques that are currently used in practical field applications. The most prevalent method currently employed in applications for damage identification in composite structural joints is ultrasonic testing [1]. The small length and time scales on which these ultrasonic elastic waves operate make them highly compatible with damage detection and localization requirements in aerospace applications. One technique currently in use in the aircraft industry is the Fokker bond method. This ultrasonic inspection method is executed in ground tests of aircraft and consists of measuring the frequency-dependent reflection coefficients of ultrasonic waves propagating through the bonded or jointed sub-structure in the megahertz frequency range [2]. This damage identification method has been successfully used in field applications for over 30 years, but it has several limitations that cause continuous in-situ structural health monitoring (SHM) to be infeasible. It is an off-line technique that requires an expert technical operator equipped with bulky test equipment and has a very limited spatial inspection range.

Several continuous SHM monitoring techniques have been developed to address the deficiencies of the off-line techniques; however, many of these method are global vibration-based damage identification schemes designed to operate at frequencies too low (wavelengths too large) to be able to identify the small changes in joint integrity that may need to

* Corresponding author.
E-mail addresses: mdtodd@ucsd.edu, mdt@ucsd.edu (M.D. Todd).

0022-460X/$ - see front matter © 2010 Elsevier Ltd. All rights reserved.
doi:10.1016/j.jsv.2010.02.009

be detected [3]. Recently, the concept of *guided* ultrasonic waves has been proposed as a solution to the problem of damage localization for *in situ* health monitoring [4,5]. These guided waves are suitable for continuous monitoring, because relatively few actuators/sensors need to be used when exploiting the waveguide geometry of the structure (plates, rails, bars, etc.). Work has been done using guided waves created with air-coupled transducers [6,7] or laser vibrometry [8]. However, these are not possible to implement for the purposes of continuous health monitoring. As a result, most researchers have turned to piezoelectric actuators as an effective means of *in situ* ultrasonic damage detection [9–11].

There are several damage detection techniques and feature extraction algorithms that use ultrasonic guided waves to interrogate adhesively bonded joints. The most prevalent of these techniques include the examination of dispersion curves and attenuation coefficients [12–14] as well as reflection and transmission characteristics [15,16]. Many of these methods also apply the use of denoising via wavelet transforms to increase signal-to-noise ratio and to selectively examine individual mode propagation of sensed waveforms [17,18]. These techniques are well established and can work in certain structures with simple geometries (e.g., flat plates, beams, etc.) or on sections with constant cross-section properties in the wave propagation direction (e.g., rails or pipes). However, these methods are difficult to adopt in structures with irregular or complicated geometries due to the very complex resulting wave propagation. These basic guided ultrasonic wave damage detection methods also have a difficult time classifying size or type of damage (at least, not without highly detailed, complicated physics-based modeling) due to the inherent simplicity of the actively imparted excitation signal, which is usually a single frequency/mode short-time wave pulse. Croxford et al. discuss a method involving subtraction of a baseline (reference) signal from a test signal that may be applicable to complex geometries and describe the current state-of-the-art in guided waves for SHM [19]. Other researchers have attempted to employ bulk insonification, where an ultrasonic source is excited and the resultant long-time, or diffuse, reverberant wave field is examined to identify structural changes [20]. This method is preferable to the standard guided wave method for structures with complex boundary conditions or geometries that make tracking and analysis of a single propagating mode and its properties difficult or impossible. A graphical overview of current ultrasonic health monitoring techniques is shown in Fig. 1.

As a means of addressing the shortcomings of current guided ultrasonic wave health monitoring techniques, this study will employ a class of algorithms originally developed in the vibration (lower-frequency acoustic) domain that are based on state space analyses using auto- or cross-prediction methods. Previous works have shown that such algorithms, when used in conjunction with actively imparted chaotic excitations, can detect bolt preload loss in various test bed structures with enhanced sensitivity over traditional vibration-domain damage detection methods such as modal analysis [21,22]. Chaotic time series are inherently narrowband and deterministic. This determinism is especially useful in applying pattern recognition techniques because, for a given set of initial conditions, the chaotic time series will always be the same. Recent research has combined the benefits of chaotic excitations (which enable and enhance pattern recognition techniques) and guided ultrasonic waves (small length and time scales) for damage detection of joints via bulk insonification [23,24]. This synthesis of techniques is accomplished by shifting the energy of a low-frequency chaotic process, such as the common Lorenz signal, into the ultrasonic frequency range (>20 kHz) and launching it into the structure as a guided wave. These chaotically amplitude-modulated ultrasonic waves are imparted to a structure by a particular kind of piezoelectric actuator known as a macro fiber composite (MFC) patch and do not require a large energy input into the system. An MFC patch is

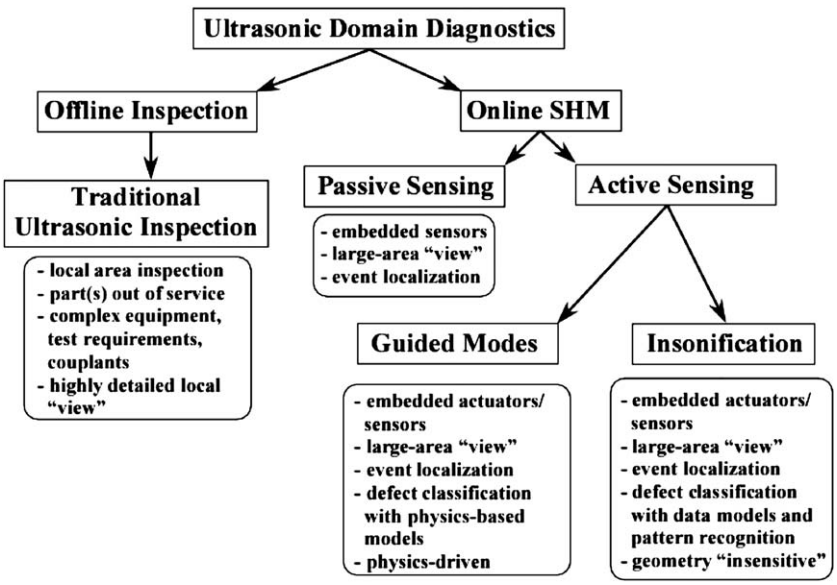

Fig. 1. Ultrasonic health monitoring paradigm.

also used to acquire the vibration response in an active sensing manner. This study uses a P2 type MFC patch that operates using a $d31$ effect that results in lateral contracting motion perpendicular to the applied electric field. The primary objective in this study is to extract a damage feature that can statistically classify the existence and type of damage present in composite wing skin-to-spar bonded joint. The proposed method applies a data-driven approach that is useful in situations where high-fidelity physics modeling is either impossible or intractable. The combination of chaotically amplitude-modulated ultrasonic insonification, time series-based pattern recognition, and a two-part novel statistical classification scheme will result in a procedure that can be used for *in situ* SHM that does not require knowledge or modeling of complex structural geometry and can classify damage existence and size.

This paper is organized in the following way. Section 2 covers the theory and background necessary for the understanding of subsequent sections. This section also details the novel two-part statistical classification scheme used in this study. Section 3 details the experimental results of three composite wing skin-to-spar test structures with different built-in damage locations and sizes. An array of signal input and feature extraction parameters are considered to determine an optimal damage detection scheme. The structures are then placed in a thermal chamber and tested at temperatures from -40 to $40\,^{\circ}$C and a method for temperature correction is established. A brief summary will then be offered in Section 4.

2. Theory and background

2.1. Signal creation

The chaotic ultrasonic waves are fundamentally created via amplitude modulation, i.e., by multiplying a single ultrasonic frequency tone by an amplitude envelope that is created by a chaotic process. A chaotic waveform is able to enhance the effectiveness of prediction error based features because the signal is deterministic. Use of a phase-randomized signal with similar frequency content results in extracted features that are not able to identify damage as well as deterministic chaotic waveforms [25,26]. The waveform appears as a narrowband, chaotically amplitude-modulated signal centered at the same central frequency as the original ultrasonic tone.

The interrogating waveform y_n is created by simple amplitude modulation of an ultrasonic carrier

$$y_n = \sin(2\pi n f_c/f_s)(1+dx_n) \tag{1}$$

where y_n is the modulated waveform, f_s is the sampling frequency (4 MHz for a high-fidelity waveform in this work), f_c is the desired carrier frequency (in the hundreds of kHz in this work), d is the modulation depth, x_n is a chaotic waveform produced by a separate chaotic process and n is the time index. Thus, the waveform x_n appears as a narrowband, chaotically amplitude-modulated signal centered at the desired central carrier frequency, f_c. In this work, the chaotic process was obtained as the x_1 output of the well-known Lorenz system

$$\begin{aligned} \dot{x}_1 &= 10(x_2-x_1) \\ \dot{x}_2 &= (-x_1x_3+28x_1-x_2) \\ \dot{x}_3 &= (x_1x_2-8x_3/3) \end{aligned} \tag{2}$$

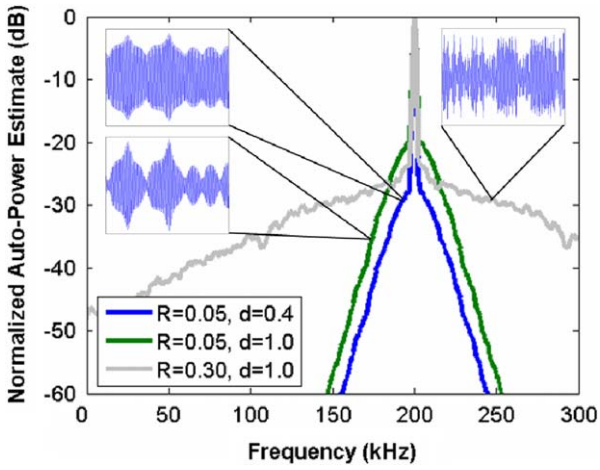

Fig. 2. Modulated chaotic signal power spectral density and time series using $R=0.05$ and $d=0.4$ (upper left), $R=0.05$ and $d=1.0$ (mid left), and $R=0.30$ and $d=1.0$ (upper right).

There is nothing unique about the Lorenz system for generating chaotic output; any system capable of producing a chaotic output is suitable, but the Lorenz system shown in Eq. (2) has a robust parameter region for producing chaotic output and was selected for this study. Eq. (2) is integrated using a time-step R/f_s, where R is the frequency ratio that can be modified to change the fundamental time scales of the chaotic signal. For this study, we use several values of R that affect the frequency regime in which the power of the chaotic signal lies. This chaotic signal is normalized through division by the maximum of the absolute value of the signal so that the values range from -1 to 1. The modulation depth d controls signal's bandwidth, and if it is greater than one, the resulting signal will be over-modulated and will result in a phase inversion at the points where $|d^*x_n| > 1$. These phase inversions would be detrimental to any prediction algorithm, and d is therefore restricted to the range $0 < d \leq 1$. Fig. 2 shows the effect of changing the frequency ratio R and the modulation depth d on the power spectral density and time series of the interrogating wave. The effectiveness of the damage detection technique used in this study is highly dependent on carrier frequency and frequency ratio but appears to be relatively insensitive to modulation depth [27].

2.2. Feature extraction

The chaotically amplitude-modulated wave has now been produced and is applied to the structure using an MFC patch. This guided wave travels through the composite joint and is received by a second MFC patch in a classic pitch/catch fashion. At this point in the damage detection scheme it is critical to choose what feature(s) from the measured waveform can be extracted to maximize the bond condition discernability of the SHM algorithm. In this study a two-step bond condition assessment algorithm is developed using autoregressive (AR) coefficients as the basic extracted feature for both steps. These AR coefficients are fit to the waveform that is received at the sensing MFC patch on the opposite side of the composite joint from the actuating MFC patch. The first step of the bond condition assessment algorithm determines if the bond being examined should be classified as undamaged or damaged. If the bond is determined to be damaged the second step of the algorithm will determine the extent or size of the damage based on baseline knowledge of how different disbond sizes will affect the AR coefficients.

2.2.1. Autoregressive models

Numerous times AR models have been shown to be useful in the field of structural health monitoring [28,29]. The discretely observed output time series $\mathbf{x}(n)$ is modeled with an AR model of the form

$$\mathbf{x}(n) = \sum_{i=1}^{p} \alpha_i \mathbf{x}(n-i) + \mathbf{e}(n) \tag{3}$$

where p is the order of the AR model with associated coefficients α_i and residual error $\mathbf{e}(n)$. In this study various model orders p are examined to determine the most suitable model order for this damage detection scheme. The AR coefficients are estimated through minimization of the sum-of-squared forward prediction errors [30]. All signals are normalized through division of the standard deviation of the signal before use of the AR model.

2.2.2. Modified modal assurance criterion

The first step in the bond condition assessment algorithm is based on a comparison of AR coefficient vectors. Fig. 3a shows averaged AR coefficients that are acquired using an AR model order of p=10 for three different bond conditions,

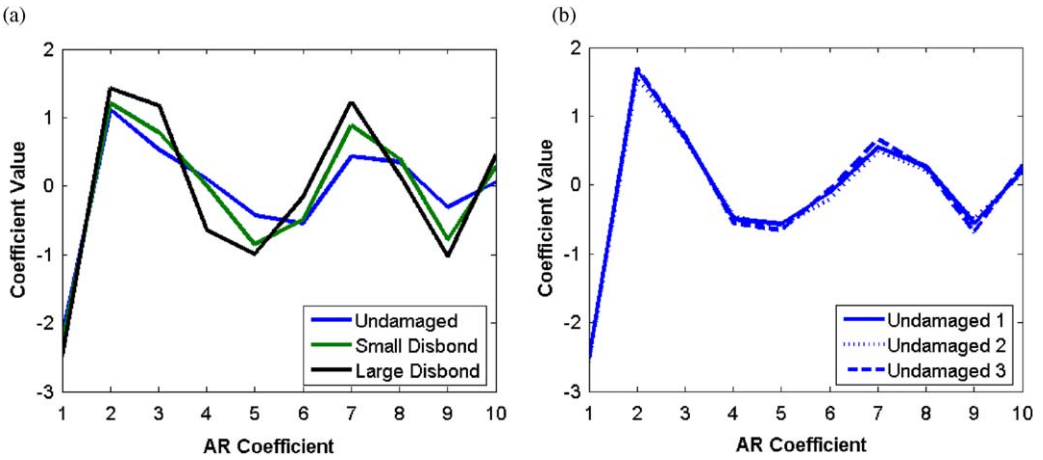

Fig. 3. Averaged AR coefficient vector comparison for (a) different bond conditions and (b) three undamaged bond conditions.

including an undamaged bond as well as two different disbond sizes on a single test structure. Fig. 3a depicts the results for one particular case, but is representative of the similarity of AR coefficient vectors from undamaged bond conditions from any single test specimen (within-unit variability). Fig. 3b shows averaged AR coefficients that are acquired using an AR model order of $p=10$ for three different undamaged bond conditions on a different test structures. The figures show a clear difference in the shape of the AR coefficient vectors for different bond conditions whereas all undamaged bond conditions result in similarly shaped AR coefficient vectors. This result suggests the use of a damage metric that compares the shape of two AR coefficient vectors.

This study proposes a feature based on the modal assurance criterion (MAC) that is commonly used in modal analysis to provide a measure of consistency between estimates of a modal vector [31]. The MAC is a scalar value detailing the linear relationship between a test modal vector and a reference modal vector as follows:

$$MAC_{tr} = \frac{|\{\psi_t\}^H\{\psi_r\}|^2}{\{\psi_t\}^H\{\psi_t\}\{\psi_r\}^H\{\psi_r\}} \tag{4}$$

where ψ_t is the test modal vector, ψ_r is the reference modal vector, and H indicates the Hermitian operator or complex conjugate. The modal assurance criterion can have values ranging from zero, representing no consistent correspondence, to unity, representing complete consistent correspondence. Therefore, if the two vectors are consistently related, then the MAC value should approach unity. This study uses a vector consistency criterion (VCC) similar to the MAC in order to measure the orthogonality of AR coefficient vectors. In this case the Hermitian operator simplifies to a vector transpose because the values of the AR coefficient vector are always real. The fact that the VCC feature can only have a value between zero and unity makes it useful as an extracted feature because scaling effects of the original signal will not affect any decision that needs to be made regarding the bond condition assessment. The hypothesis being tested is that two AR coefficient vectors should be very consistent (nearly orthogonal) if they are derived from the same bond condition model.

2.3. Step one: undamaged/damaged classification

The determination of whether a bond of unknown condition is undamaged or damaged is accomplished using the following method. First, a set of forty-five distinct 250 μs-long input signals are created from the data-generating process that has been previously described in Section 2.1. For each of these forty-five input signals a 500 μs-long structural response is recorded once under each of the known undamaged and damaged bond conditions on a particular specimen, using a different actuator/sensor pair for each bond, as well as a second time for the undamaged bond condition. AR coefficients are then estimated for each of these structural responses using the above outlined method and the first 250 ms of the sensed signal starting with the first arrival. These sets of AR coefficients form a database of structural responses for known bond conditions with each input signal that will be used to determine the bond condition of an unknown bond in a supervised learning fashion.

For the first step of the bond condition assessment algorithm, which will detect whether an unknown bond is damaged or undamaged, a distribution of VCC values is then calculated. This is accomplished by comparing, using Eq. (4), each of the forty-five AR coefficient vectors from the first set of waveforms to probe the undamaged bond with each of the forty-five AR coefficient vectors from the second set of waveforms to probe the undamaged bond. This calculation results in a distribution of 2025 VCC values that describe the auto-correlation between the two sets of AR coefficient vectors that are both derived from the undamaged bond condition. Forty-five new input signals (created from the same underlying process as the supervised learning database input signals) are then applied to the structure along an unknown bond condition path. AR coefficient vectors are again calculated for each of these new structural responses. The forty-five AR coefficient vectors from the original undamaged bond condition are then compared with the new set of forty-five AR coefficient vectors from the unknown bond condition by calculating VCC values. This computation results in a distribution of 2025 VCC values that describe the correlation between the AR coefficient vectors of the undamaged bond condition and the AR coefficient vectors of the unknown bond condition.

2.3.1. Statistical classification

A statistical measure must now be devised that can properly classify a damaged bond and at the same time properly classify an undamaged bond in a different geometric locations using a different MFC sensor/actuator pairs than the baseline undamaged bond. Fig. 4a shows empirical probability distribution functions (pdfs) of VCC values for three different bond conditions, including an undamaged bond as well as two different disbond sizes. Fig. 4b shows empirical pdfs of VCC values for three different undamaged bond conditions in different geometric locations on the same test structure. It is clear that while there are differences in the pdfs of the undamaged bonds in Fig. 4b that the difference between the pdfs of the undamaged bond and two disbond sizes in Fig. 4a are much greater. A statistical decision boundary that can account for the small differences in the pdfs due to geometric conditions as well as MFC bonding characteristics while still correctly classifying the damaged bonds would be beneficial. The pdfs are not normally distributed as can be seen from the elongated left tail. Therefore, standard statistical tests that assume normality such as the Student's t-test cannot be used in this case. There are several non-parametric tests that can be employed for non-Gaussian distributions such as the Kolmogorov–Smirnov test or the Mann–Whitney U test, but in this study these tests classify the various

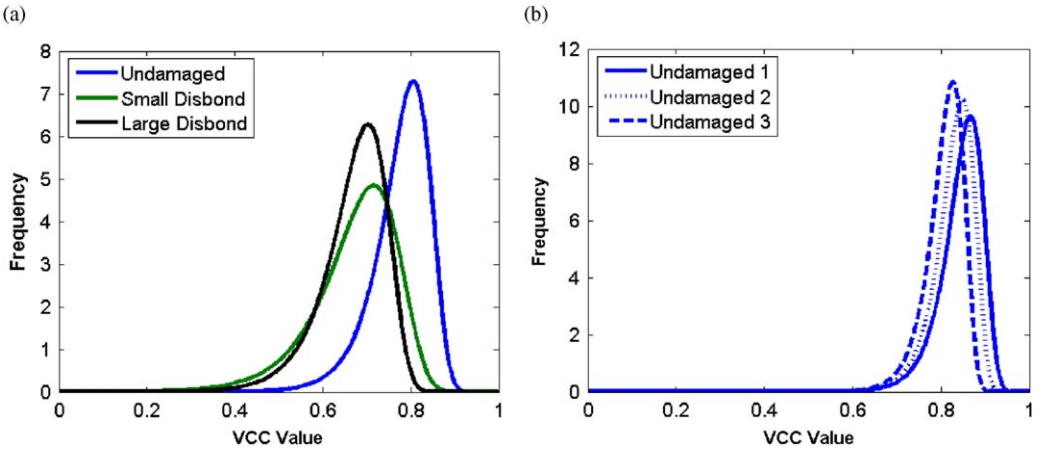

Fig. 4. MAC value empirical pdf comparison for (a) different bond conditions and (b) three undamaged bond conditions.

undamaged pdfs as being from different parent distributions. A solution to this problem is to set a lower confidence limit on an undamaged pdf so that the other undamaged pdfs would not result in a significant number of outliers (VCC values less than the lower bound) but still produce a significant number of outliers for the damaged pdfs.

2.3.2. Extreme value statistics

Extreme value statistics (EVS) are used to set the lower confidence limit on the non-normal distributions that are produced using the above outlined method. EVS is used in this analysis to accurately model the behavior of the feature distribution's tails. The basis of this branch of statistics stems from the following situation. If a moving window is taken along a vector of samples and the minimum value is selected from each of these windows, the induced cumulative density function of the minima of the samples, as the number of vector samples tends to infinity, asymptotically converges to one of three possible distributions: Gumbel, Weibull, or Frechet [32].

$$\text{Gumbel}: \quad F(x) = 1 - \exp\left[-\exp\left(\frac{x-\lambda}{\delta}\right)\right] \quad -\infty < x < \infty \quad \text{and} \quad \delta > 0 \tag{5}$$

$$\text{Weibull}: \quad F(x) = \begin{cases} 0 & \text{If } x \le \lambda \\ 1 - \exp\left[-\left(\frac{x-\lambda}{\delta}\right)^{\beta}\right] & \text{otherwise} \end{cases} \tag{6}$$

$$\text{Frechet}: \quad F(x) = \begin{cases} 1 - \exp\left[-\left(\frac{\delta}{\lambda-x}\right)^{\beta}\right] & \text{If } x \le \lambda \\ 1 & \text{otherwise} \end{cases} \tag{7}$$

where λ, δ, and β are the model parameters that are estimated from the data. These same functions also apply to the converged distributions for the maxima of the sample sets.

The appropriate distribution is chosen by plotting the cumulative distribution function (cdf) of the extracted vector of minima on the probability paper for a Gumbel distribution. This probability paper is designed so that the cdf will plot in a linear fashion if the vector of minima has a Gumbel minimum distribution. Otherwise, the cdf will have an associated curvature. If this curvature is concave, the feature vector has a Weibull minimum distribution. Similarly, if the curvature is convex the feature vector has a Frechet minimum distribution. In this study the distribution of minima taken from the parent undamaged VCC distributions has a Gumbel minimum distribution. Model parameters are then estimated by fitting the chosen distribution to the data as outlined in [32].

Once the model parameters are chosen, it is possible to generate confidence limits that can be applied to the distribution. These limits are far more accurate than those obtained when assuming a Gaussian distribution. The threshold corresponding to a specific confidence level for the Gumbel minimum distribution is given by the following equation [33]:

$$\text{Gumbel}: \quad x_{\min} = \lambda + \delta \ln\left[-\ln\left(1 - \frac{n\alpha}{2}\right)\right] \tag{8}$$

where n is the window size used to extract the maxima, and α is the associated Type I error of the confidence limit. Type I error is simply the percentage of false positives that are expected to appear. For example, when using a 95% confidence interval the Type I error is expected to be 5% (α=0.05). By using the confidence limit calculated through EVS the bond state assessment algorithm is able to differentiate between undamaged and damaged paths. To further differentiate between different sizes of disbonds a second classification scheme is used.

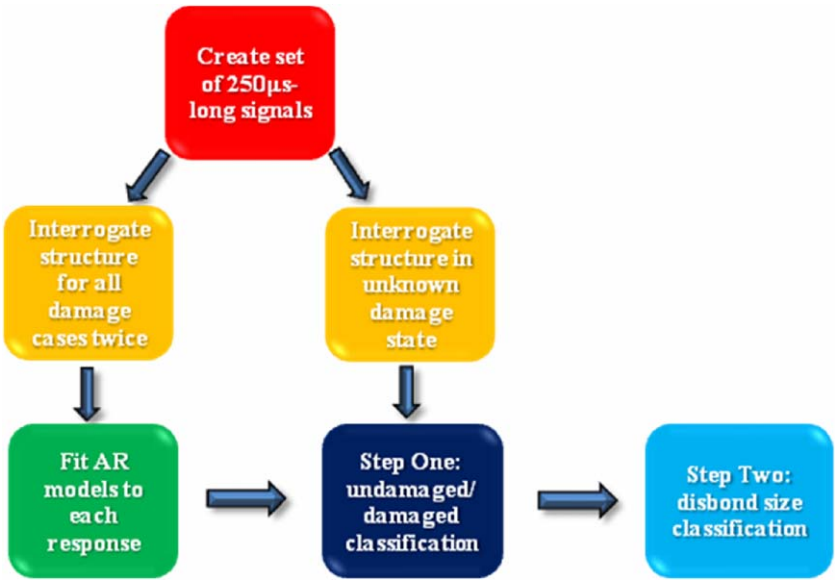

Fig. 5. Ultrasonic statistical classification paradigm.

2.4. *Step two: disbond size classification*

A novel statistical classification technique with its basis in information theory is used to classify different disbond sizes in this study. The classification method is based on a fundamental theorem of Shannon's information theory that states that "the best compression for any given data set comes from a codebook designed exactly for the statistics of that source; any other codebook will give worse results" [34]. Recently information theory has been applied to continuous time signals, where compression performance is related to prediction error, and a codebook is the model for a source that produces time series data. In this study, the source is guided waves propagating through a composite bond. These time series can then be classified using prediction error as a means of virtual data compression (via the AR coefficient vectors). The model for the response time series is the same autoregressive model used for the undamaged/damaged discrimination that has already taken place. This idea leads to a procedure for classifying time series using cross-prediction error, as literal "data compression" in the sense of maximal information recovery on decompression is not actually necessary, just its "virtual" performance as a representative data model. Of course, the better the underlying statistical model is the more the classification performance will improve.

The entire disbond size classification technique can be summarized as follows. The same database of AR coefficients that was created using forty-five chaotically amplitude-modulated ultrasonic guided waves is again used to decide the size of the disbond. In this case only AR coefficients from the damaged paths are used because it is now known that the test path has some form of damage after using the first classification technique. A new input signal (created from the same underlying process as the training database input signals) is then applied to the structure along the known damaged bond condition path. One of the forty-five sets of AR coefficients in the training database for each of the paths with disbond damage are then used to estimate the structural response to the new input signal. One set of coefficients from the training database will minimize the sum of the squared residual errors and these coefficients are associated with a known disbond size in the training database. This disbond size is then classified as the size of the unknown disbond that is being probed. This comparison then takes place for each of the remaining forty-five input signals in the training database. This entire process is then repeated using forty-five input signals that are imparted to the structure in its unknown bond condition state (the same data as was used in the first classification step). The votes for each bond condition are then summed and the condition and the plurality of votes is the estimated condition of the bond. The statistical classification paradigm can be shown visually as in Fig. 5.

3. Experimental investigation

Previous work has shown the ability of the above outlined disbond size classification method to detect and classify bolt preload level in a single bolt aluminum lap joint as well as a multiple bolt aluminum frame structure [35] and in a composite wing-to-spar adhesive bonded joint [36]. In this study the disbond size classification technique is combined

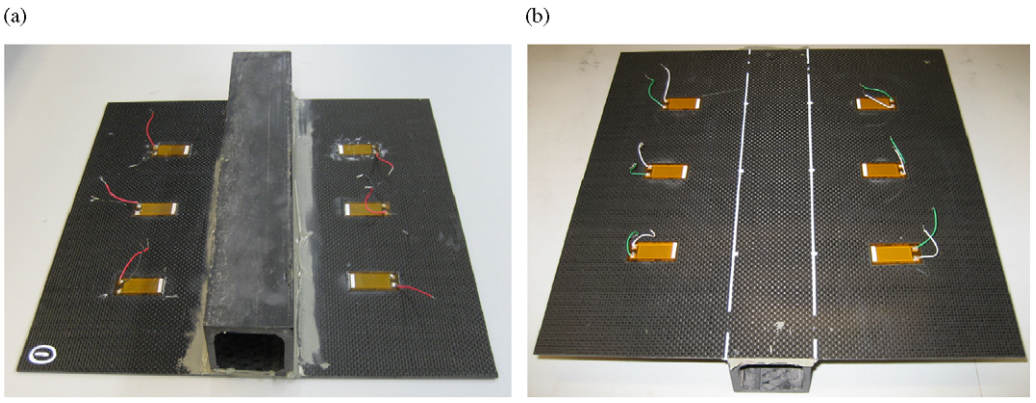

Fig. 6. Experimental platform showing location of bottom-mounted MFC actuators on Plate 1 (a) and top-mounted MFC actuators on Plate 2 (b).

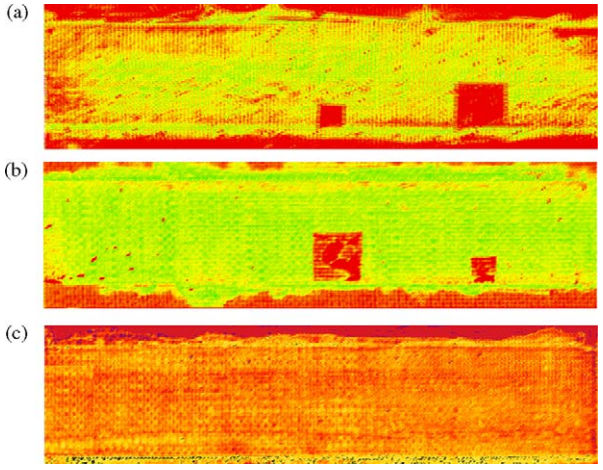

Fig. 7. C-scan images showing locations and sizes of disbonds for Plate 1 (a) and Plate 2 (b) as well as undamaged Plate 3 (c).

with the damage/undamaged classification method and applied to three composite wing-to-spar adhesive bonded joints. The test structures consist of a carbon fiber-reinforced plastic (CFRP) plate (manufactured by McMaster-Carr) that is bonded to a tubular CFRP spar using Loctite® Hysol® 9462 'Two Component Epoxy Adhesive'. The CFRP plate measures 0.3 m × 0.3 m × 4 mm square and the spar has an outer square diameter of 0.5 × 0.5 m with a wall thickness of 6 cm. The bonded area for two of the specimens contains two different sizes of disbond (1.6 and 6.4 cm^2) that are created using Teflon. The structures with disbonds are labeled Plates 1 and 2. The third test structure (Plate 3) was manufactured with no disbonds so all paths are undamaged and geometric effects can be studied. The locations of the MFC actuators/sensors for Plates 1 and 2 are pictured in Fig. 6. C-scans that depict the bond state of each specimen can be seen in Fig. 7.

Plate 1 features two MFC actuator/sensors are attached to the CFRP plate on each side of the bond for both of the damaged bond states as well as one pair for the undamaged bond area for a total of six MFC patches. The MFC patches are located on the spar side of the bond as seen in Fig. 6. The MFC patches on Plate 2 are located on the opposite side of the CFRP plate from the bonded area. Plate 3 also has six MFC patches that are bonded on the spar side of the structure, as in Plate 1. Each of these Smart Material Corporation MFC patches (M 2814 P2) have an active area of 28 × 14 mm, are approximately 0.3 mm thick and are bonded to the structure using Loctite® Hysol® E120HP™ epoxy adhesive. Each MFC patch is affixed to the structure at a distance of 20 mm from the spar bond line. Each input signal is applied to the structure 25 times and then averaged and filtered to reduce experimental noise. The actuation signal is created by the output channel of a National Instruments PCI-6110 DAQ card at a rate of 4 MHz and routed through a Krohn-Hite 7602 wideband power amplifier. This amplified signal is sent to the actuation MFC while the sensing MFC simultaneously samples the structural response at the rate of 4 MHz.

3.1. Optimal parameter investigation

A preliminary study is undertaken to determine the set of input signal parameters and extracted feature parameters (such as AR model order) that produce optimal bond state identification. The bond state assessment algorithm is used for

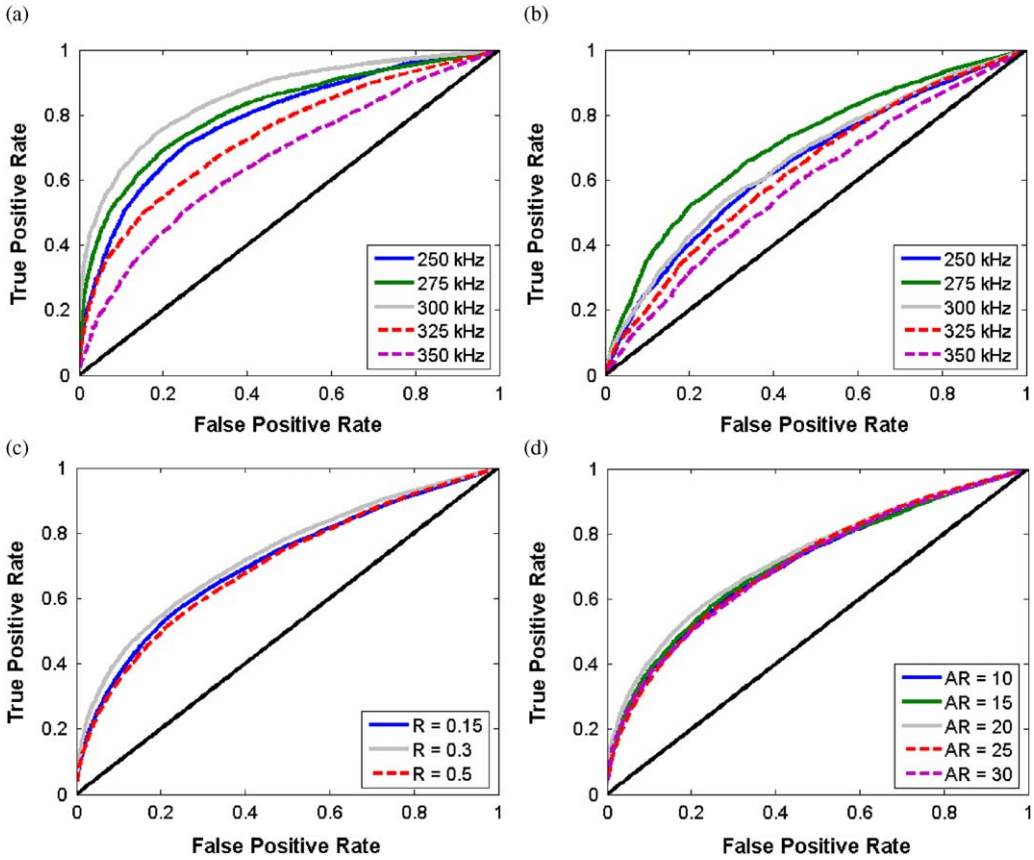

Fig. 8. ROC curves for (a) Plate 1 center frequencies, (b) Plate 2 center frequencies, (c) Plate 1 frequency ratio R and (d) Plate 1 AR model order.

an array of signal parameters and the overall ability of each set of parameters to correctly identify each bond state is then examined. In this study a number of excitation center frequencies from 100 to 350 kHz are considered, as well as frequency ratios ranging from 0.15 (slightly chaotic) to 0.50 (highly chaotic). When considering the feature extraction parameters a number of AR model orders from 10 to 30 were employed. Fig. 8a–d depicts the ability of the VCC-/EVS-based statistical classification scheme to correctly identify bond condition by plotting the receiver operating characteristic (ROC) curve. This plot depicts the true positive rate against the false positive rate for all possible classifications (both undamaged and damaged). Essentially the more area under a ROC curve is the better job of correctly identifying bond state what particular parameter is doing because there will be a high number of true positives compared to a low number of false positives (Type I error).

Fig. 8a shows various ROC curves acquired by changing the center frequency of the excitation signals on Plate 1. Performance of the bond state assessment algorithm increases from a center frequency of 100 up until 300 kHz, at which point the performance degrades as the center frequency continues to increase to 350 kHz (only center frequencies from 250 to 350 kHz are shown here). This means that for the particular geometry of the test specimen and with MFC patches affixed to the same side of the plate as the bond line that a center frequency of 300 kHz is best suited for bond state assessment. Fig. 8b depicts the same change in center frequencies as Fig. 8a except that the data is from Plate 2 which has the MFC patches bonded on the opposite side of the bonded spar. There is similar behavior to the previous plot in which performance increases from 100 kHz to a particular optimal frequency and then decreases again. However, in this case the optimal center frequency is 275 kHz. This change is due to the different ways the guided wave propagates through the bond when introduced to the plate on the opposite side of the spar.

Fig. 8c shows the ability of the statistical classification scheme employed together with chaotic insonification to correctly identify bond condition for various frequency ratios on Plate 1. As previously mentioned, the lower the frequency ratio the more sinusoidal the input signal appears and conversely the higher the frequency ratio the more chaotic the input signal appears. This signal parameter characteristic occurs because as the frequency ratio becomes small, the chaos operates on a longer time scale. If a small enough time window is used to create the signal, a very small R value will result in the chaotic time scale being much longer than that of the entire signal. In this case the signal will appear to be almost sinusoidal. The opposite effect holds true if a large frequency ratio is used because the time scale of the chaos operates on

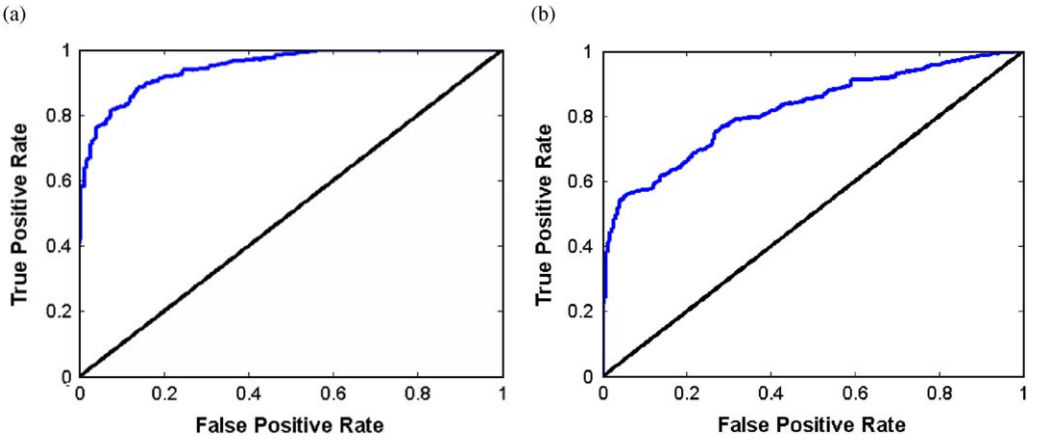

Fig. 9. Optimal ROC curves for (a) Plate 1 and (b) Plate 2.

will be much smaller than the length of the signal and the signal will, therefore, contain more chaotic information. A frequency ratio of 0.3 appears to be best suited for bond state assessment. The ROC curves for Plate 2 frequency ratios are very similar and again show that a frequency ratio of 0.3 is optimal. Fig. 8d depicts the effect of AR model order on the damage identification ability of the statistical classification scheme. All AR model orders appear to work approximately equally well, with an AR model order of 20 performing the best among the group. Again Plate 2 shows similar results for the AR model order. There is likely a physical explanation for each of these optimal parameters but determining the exact physics behind this result is beyond the scope of this paper. It is not possible to create any ROC curve for Plate 3 as there are no true positive results because there is no damage (and thus, no hypothesis test). Fig. 9 shows the optimal ROC curve for Plates 1 and 2.

3.2. Temperature variability

3.2.1. Step one: undamaged/damaged classification

The experimental apparatus used in this study is meant to simulate a wing skin-to-spar bonded joint that is used in aerospace applications. If this bond state assessment algorithm is to be used for *in situ* health monitoring, including in-flight and on the ground, its behavior and effectiveness relative to external temperature must be considered. This study uses a thermal chamber to test the efficacy of the above outlined method for temperatures varying from -40 to 40 °C, a range that covers most flight and ground conditions. The optimal set of parameters that will be used in the following experiments is a center frequency of 300 kHz for Plates 1 and 3 (MFC patches on the same side as the bond) and a center frequency of 275 kHz for Plate 2 (MFC patches on the opposite side as the bond). A frequency ratio of 0.3 will be used for all specimens as well as an AR model order of 20. An alpha level of 0.05 (5% type I error) is used to choose the lower confidence limit for the undamaged MAC distribution. Fig. 10a and b shows the percentage of outliers for each bond state being inspected on Plates 1 and 2, respectively. This percentage of outliers is plotted against temperature and the "training database" of AR coefficient vectors has been acquired at each temperature. If the percentage of outliers is above the 5% type I error that has been specified the bond state assessment algorithm has determined that the unknown bond being inspected is damaged.

Fig. 10a and b shows that for every temperature the undamaged path and paths with disbonds are correctly classified, because the blue undamaged line is always below the decision boundary and the red and green disbond lines are always above the decision boundary. It is, therefore, possible to correct for temperature variations by storing baseline AR coefficients for the range of temperatures that the intended apparatus is likely to see during real world applications. However, it is not necessary to store AR coefficients for all possible temperatures because only a few temperatures need to be stored and AR coefficients for intermediate temperatures can be linearly interpolated between existing baseline AR coefficients. This study examines using baseline AR coefficients taken every 20 °C (-40, -20, 0, 20, and 40 °C) which is referred to in the following figures as 5tempbase and using baseline AR coefficients taken every 10 °C (-40, -30, -20, -10, 0, 10, 20, 30, and 40 °C) which is referred to in the following figures as 9tempbase. Testing was carried out at 5 °C temperature increments. Fig. 11 shows that the value of each AR coefficient changes smoothly and monotonically in nearly a piece-wise linear fashion as the temperature changes. This result makes it possible to store AR coefficients from only a few temperatures and linearly interpolate new AR coefficients at all other temperatures.

Fig. 12a and b depicts the same results as seen in Fig. 10b except that AR coefficient values are linearly interpolated at temperatures for which no baseline data is present. The 5tempbase method depicted in Fig. 12a works well except for two

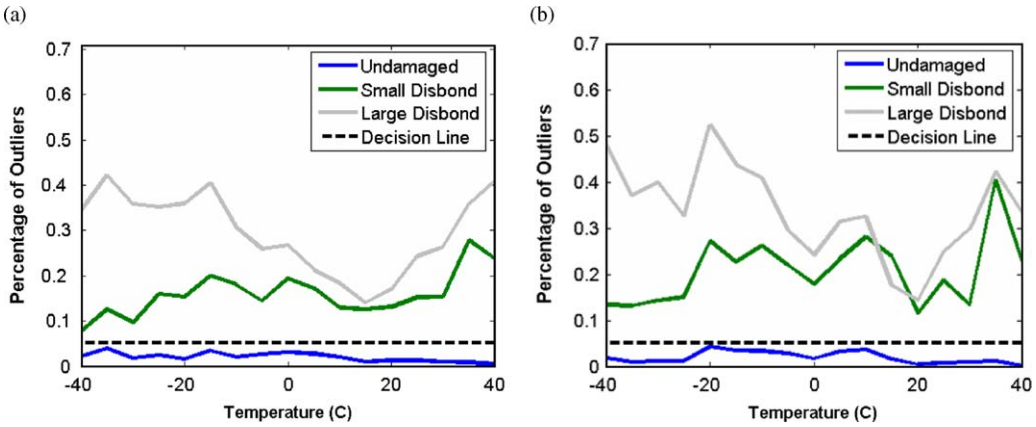

Fig. 10. Percentage of outliers vs. temperature for each bond condition on (a) Plate 1, (b) Plate 2.

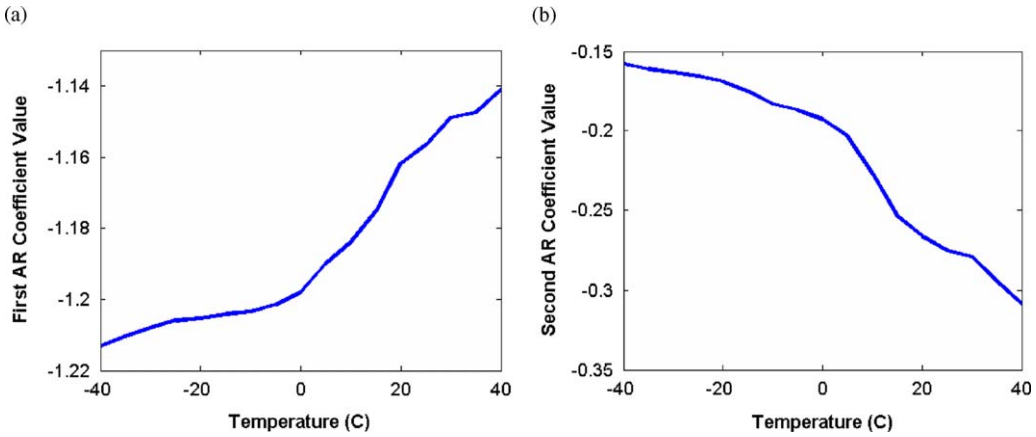

Fig. 11. Actual coefficient values vs. temperature for the first (a) and second (b) AR coefficients of the undamaged condition on Plate 2 using an AR model order of 20.

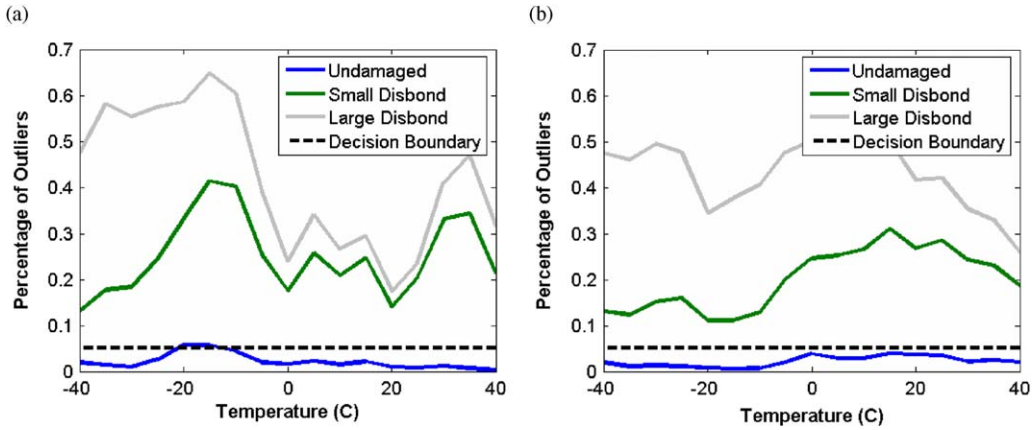

Fig. 12. Percentage of outliers for Plate 2 using the 5tempbase (a) and 9tempbase (b) methods of AR coefficient interpolation.

temperatures at which the number of outliers for the undamaged path rises above the critical threshold. The 9tempbase method shown in Fig. 12b has 100% correct classification at all temperatures. This study, therefore, concludes that the best method for temperature correction is to store baseline coefficients for a small number of temperatures that span the known operational values of the structure and then to linearly interpolate, via a lookup table, the AR coefficients necessary to correctly classify bond condition for any intermediate temperatures.

3.2.2. Step two: disbond size classification

Having already determined what paths have some form of disbond or damage, the second bond state assessment algorithm employed in this study seeks to classify the size of the disbond. Fig. 13 shows the percentage of total correct votes for each disbond size using either the 5tempbase or 9tempbase AR coefficient interpolation method for Plates 1 and 2. The 5tempbase and 9tempbase methods appear to work equally well and the large disbond is correctly identified in almost 100% of individual cases. The small disbond is occasionally misclassified but the lowest result at 15 °C on Plate 2 is still greater than 90% correct classification.

3.3. Other sources of variability

The previous section showed the ability of the bond state assessment algorithm outlined in this study to compensate for temperature variations (variability due to the environment). Other types of variability that could affect the outcome of this scheme include unintentional inhomogeneities in a single manufactured specimen ("within-unit" variability) and inconsistencies in the manufacturing process itself across specimen lots ("unit-to-unit" variability). Within-unit variability includes the effects of manufacturing variability along the bond line, MFC bond condition inconsistency, and geometric effects that result from different placements of the MFC sensor/actuator pairs. It is possible to observe the resulting effects of within-unit variability by examining Plate 3, in which all paths were undamaged. Fig. 14 shows the number of outliers using the VCC feature for Plate 3. In this figure, one path was chosen to be the baseline undamaged path and the other two paths were used as test cases. The number of outliers for each of the two test undamaged paths is above the 5% threshold but are less than 7.5% and much less than the number of outliers seen in the paths with disbonds on Plates 1 and 2 shown in Fig. 10a and b. This result only comes from one test structure, but it appears that it may be possible to build a safety factor (in this case 1.5) into the lower confidence limit to account for the various sources of within-unit variability on a

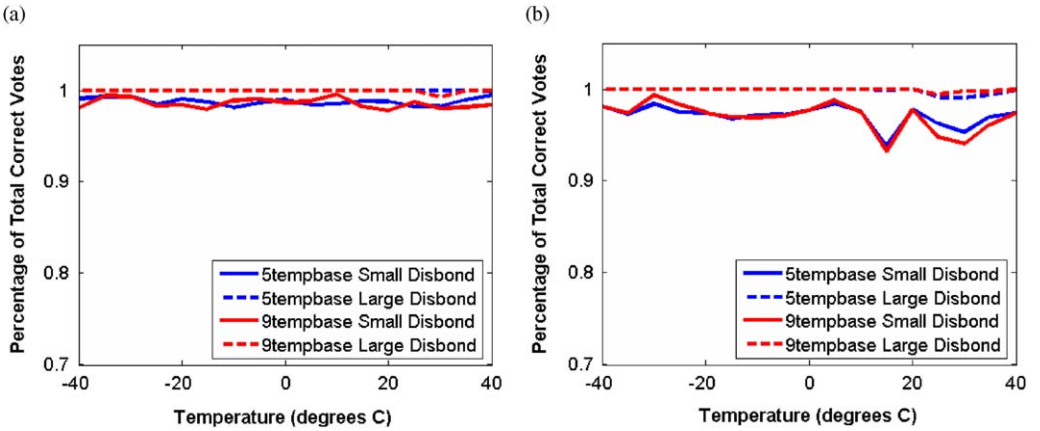

Fig. 13. Percentage of total correct votes for each disbond size using the 5tempbase and 9tempbase AR coefficient interpolation methods on Plate 1 (a) and on Plate 2 (b).

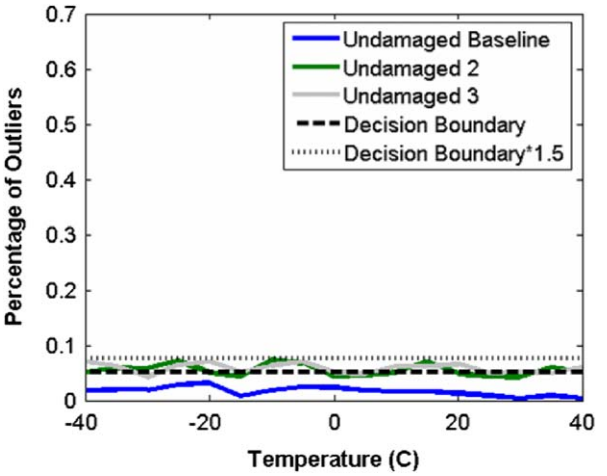

Fig. 14. Percentage of outliers vs. temperature for each bond condition on Plate 3.

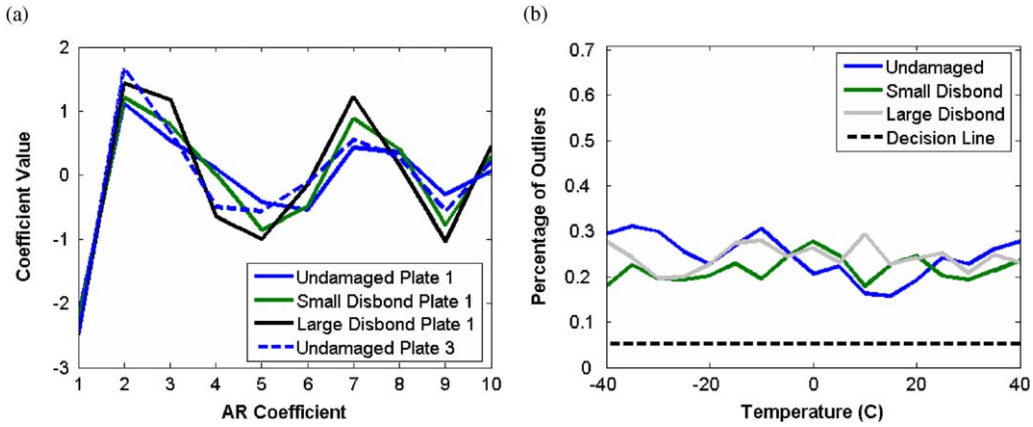

Fig. 15. Averaged AR coefficient vector comparison for each bond condition on Plate 1 vs. undamaged bond condition on Plate 3 (a). Percentage of outliers vs. temperature for each bond condition on Plate 1 using undamaged bond condition on Plate 3 as the undamaged baseline (b).

particular structure and still be able identify when and where the state of the bond has been changed. This result is important, because it means it may not be necessary to store baseline data for every MFC actuator/sensor pair in a structure as it may be possible to generalize baseline data from elsewhere in the structure as long as the geometries are similar.

Unit-to-unit variability arises due to inconsistent manufacturing processes from specimen to specimen. In well-controlled automated industrial applications with very tight tolerances or requirements, unit-to-unit variability is typically lower than within-unit variability. However, in this study each specimen was manufactured individually by hand, and consequently the unit-to-unit variability is considerably larger than within-unit variability. Fig. 15 illustrates the large effect of this manufacturing inconsistency. Fig. 15a shows averaged AR coefficients that are acquired using an AR model order of $p=10$ for the three different bond conditions on Plate 1 and the undamaged bond condition on Plate 3 that is in the same geometric location as the undamaged bond condition on Plate 1. Inspection of Fig. 15a reveals that the AR coefficient vector from the undamaged bond condition on Plate 3 differs as much from the AR coefficient vector from the undamaged bond condition on Plate 1 as the AR coefficient vectors from the two disbond conditions on Plate 1. This large difference between the AR coefficient vectors from the undamaged bond condition in the same geometric location on each plate shows that the unit-to-unit variability is too large to use baseline data gathered on one specimen to discern the damage state of a second specimen. This conclusion is depicted graphically in Fig. 15b, which shows the percentage of outliers vs. temperature for each bond state on Plate 1 using the undamaged bond condition on Plate 3 as the baseline undamaged condition. The percentage of outliers for the undamaged bond condition on Plate 1 is well above the decision boundary and would therefore be classified as damaged if the undamaged bond condition from Plate 3 were used as a baseline. Thus it is concluded that for the manufacturing techniques used in this study (individual test specimen construction by a non-expert human technician) that unit-to-unit variability is too large to allow for baseline data gathered from one plate to be used to diagnose the bond condition of a second plate. This result does not preclude the possibility that with more controlled manufacturing processes that unit-to-unit variability could be small enough that baseline data from only one specimen would be needed to properly assess the bond condition of a specimen lot.

4. Summary

This study has shown the ability of a new two-part bond state assessment algorithm to correctly classify the existence and size of a disbond within a composite bonded wing skin-to-spar structure. Chaotically amplitude-modulated ultrasonic waves are imparted to the composite structure through a piezoelectric patch, with a second piezoelectric patch recording the subsequent structural response. This structural response is modeled using an autoregressive (AR) model and the resulting AR coefficients are the basic extracted feature used to classify the bond state. The use of vector consistency criterion (VCC) values derived from comparison of AR coefficient vectors, in combination with outlier analysis based on extreme value statistics, allows undamaged/damaged classification to be possible, even without baseline data from every MFC sensor/actuator pair in a structure. Disbond size can be determined in a supervised learning manner by employing a classification technique derived from elements of information theory. This method also has the ability to compensate for temperature variability provided baseline AR coefficients have been recorded at a suitable number of temperatures that span the operating range of the structure (and, of course, that temperature is measured *in situ* during operation). This method has the ability to detect and locate small levels of damage due to the frequency regime of the excitation signal. It will be preferable to standard ultrasonic SHM techniques that examine dispersion curves, wave attenuation, and reflection characteristics for specific applications because it is able to locate and classify different disbond sizes even for complicated geometries.

However, further work must be completed to examine the effect that dynamic loading of the structure during in-service conditions will have on the efficacy of this method. This study also did not address the matter of how close MFC actuators need to be placed to the bond line to be able to detect damage. In this research the optimal choice of parameters that affect the creation of the input time signals (carrier frequency f_c, frequency ratio R, and modulation depth d) as well as feature extraction (AR model order, size of training and test databases) is determined by examining a range of values for each of these parameters. It may be possible to use genetic programming to determine a global optimum parameter solution that was not found by only testing a few finite parameter vectors. Using genetic algorithms (specifically differential evolution) to create an optimal input waveform for maximum damage discernment has already been investigated [24]. This method showed significant improvement (two orders of magnitude) in solution 'fitness' over a random set of input parameters.

Acknowledgements

This work is also primarily supported by the Air Force Office of Scientific Research (Dr. Victor Giurgiutiu, Program Manager) under contract #FA9550-07-1-0016. Other support was given by the UCSD/Los Alamos National Laboratory Engineering Institute for Structural Health Monitoring, Damage Prognosis, and Validated Simulations (Dr. Charles Farrar, Director). The authors acknowledge Dr. Matt Kennel of Fair-Isaac Inc. for the helpful technical discussion.

References

[1] C.H. Guyott, P. Cawley, R.D. Adams, The non-destructive testing of adhesively bonded structures, *Journal of Adhesion* 20 (1986) 129–159.
[2] C.H. Guyott, P. Cawley, Evaluation of cohesive properties of adhesive joints using ultrasonic spectroscopy, *NDT International* 21 (1988) 233–240.
[3] S.W. Doebling, C.R. Farrar, M.B. Prime, D.W. Shevitz, Damage identification and health monitoring of structural and mechanical systems from changes in their vibration characteristics: a literature review. *Los Alamos National Laboratory Report* LA-13070-MS, 1996.
[4] D.N. Alleyne, M.J.S. Lowe, P. Cawley, The inspection of chemical plant pipework using Lamb waves: defect sensitivity and field experience, in: D.P. Thompson, D.E. Chimenti (Eds.), *Review of Progress in Quantitative Nondestructive Evaluation*, Plenum, New York, 1996, pp. 1859–1866.
[5] P.D. Wilcox, M.J.S. Lowe, P. Cawley, Long range Lamb wave inspection: the effect of dispersion and modal selectivity, in: D.P. Thompson, D.E. Chimenti (Eds.), *Review of Progress in Quantitative Nondestructive Evaluation*, Plenum, New York, 1996, pp. 151–158.
[6] M. Castaings, P. Cawley, R. Farlow, Air-coupled ultrasonic transducers for the detection of defects in plates, in: D.P. Thompson, D.E. Chimenti (Eds.), *Review of Progress in Quantitative Nondestructive Evaluation*, Plenum, New York, 1996, pp. 1083–1090.
[7] D. Tuzzeo, F. Lanza di Scalea, Non-contact air-coupled ultrasonic guided waves for detection of thinning defects in aluminum plates, *Research in Nondestructive Evaluation* 13 (2) (2001) 61–78.
[8] W.J. Staszewski, B.C. Lee, L. Mallet, F. Scarpa, Structural health monitoring using scanning laser vibrometry: I. Lamb wave sensing, *Smart Materials and Structures* 13 (2) (2004) 251–260.
[9] V. Giurgiutiu, A. Zagrai, Embedded self-sensing piezoelectric active sensors for on-line structural identification, *ASME Journal of Vibration and Acoustics* 124 (2002) 116–125.
[10] J.R. Wait, G. Park, H. Sohn, C.R. Farrar, Plate damage identification using wave propagation and impedance methods, *Proceeding of the SPIE Seventh Annual International Symposium on NDE for Health Monitoring and Diagnostic,* vol. 5394, San Diego, CA, March 2004, pp. 53–65.
[11] V. Giurgiutiu, Tuned Lamb wave excitation and detection with piezoelectric wafer active sensors for structural health monitoring, *Journal of Intelligent Materials Systems and Structures* 16 (2005) 291–305.
[12] P.C. Xu, A.K. Mal, Y. Bar-Cohen, Inversion of leaky Lamb wave data to determine cohesive properties of bonds, *International Journal of Engineering Science* 28 (1990) 331–346.
[13] A. Pilarski, J.L. Rose, Lamb wave mode selection concepts for interfacial weakness analysis, *Journal of Nondestructive Evaluation* 11 (1992) 237–249.
[14] R. Seifried, L.J. Jacobs, J. Qu, Propagation of guided waves in adhesive bonded components, *NDT&E International* 35 (2002) 317–328.
[15] S.I. Rokhlin, Lamb wave interaction with lap-shear adhesive joints: theory and experiment, *Journal of the Acoustical Society of America* 89 (1991) 2758–2765.
[16] M.J.S. Lowe, P. Cawley, Applicability of plate wave techniques for the inspection of adhesive and diffusion bonded joints, *Journal of Nondestructive Evaluation* 13 (1994) 185–200.
[17] A. Abbate, J. Koay, J. Frankel, S.C. Schroeder, P. Das, Signal detection and noise suppression using a wavelet transform signal processor: application to ultrasonic flaw detection, *IEEE Transactions on Ultrasonics, Ferroelectrics, and Frequency Control* 44 (1997) 14–26.
[18] F. Lanza di Scalea, P. Rizzo, A. Marzani, Propagation of ultrasonic guided waves in lapshear adhesive joints: case of incident a0 Lamb wave, *Journal of the Acoustical Society of America* 115 (1) (2004) 146–156.
[19] A.J. Croxford, P.D. Wilcox, B.W. Drinkwater, G. Konstantinidis, Strategies for guided-wave structural health monitoring, *Proc. Roy. Soc. A* 463 (2087) (2007) 2961–2981.
[20] J.E. Michaels, T.E. Michaels, Detection of structural damage from the local temporal coherence of diffuse ultrasonic signals, *IEEE Transactions on Ultrasonics, Ferroelectrics, and Frequency Control* 52 (2005) 1769–1782.
[21] J.M. Nichols, M.D. Todd, J.R. Wait, Using state space predictive modeling with chaotic interrogation in detecting joint preload loss in a frame structure experiment, *Smart Materials and Structures* 12 (4) (2003) 580–601.
[22] M.D. Todd, K. Erickson, L. Chang, K. Lee, J.M. Nichols, Using chaotic interrogation and attractor nonlinear cross-prediction error to detect fastener preload loss in an aluminum frame, *Chaos: An Interdisciplinary Journal of Nonlinear Science* 14 (2) (2004) 387–399.
[23] T.R. Fasel, M.D. Todd, G. Park, Piezoelectric active sensing using chaotic excitations and state space reconstruction, *Proceedings of the SPIE Tenth Annual International Symposium on NDE for Health Monitoring and Diagnostics,* vol. 5768, San Diego, CA, March 2005, pp. 253–263.
[24] T.R. Fasel, M.D. Todd, G. Park, Active chaotic excitation for bolted joint monitoring, *Proceedings of the SPIE Eleventh Annual International Symposium on NDE for Health Monitoring and Diagnostics,* vol. 6174, San Diego, CA, March 2006, pp. 6174S-1–6174S-8.
[25] C.C. Olson, L.A. Overbey, M.D. Todd, The effect of detection feature type on excitations bred for active sensing in structural health monitoring, *Journal of Intelligent Material Structures and Systems* 20 (2009) 1307–1327.
[26] C.C. Olson, M.D. Todd, On the convergence of multiple excitation sources to a global optimum excitation in active sensing for structural health monitoring, *Structural Control and Health Monitoring* 17 (2010) 23–47.
[27] T.R. Fasel, C.C. Olson, M.D. Todd, Optimized guided wave excitations for health monitoring of a bolted joint, *Proceedings of the SPIE Thirteenth Annual International Symposium on NDE for Health Monitoring and Diagnostics,* vol. 6935, San Diego, CA, March 2008, pp. 69351N-1–69351N-8.
[28] H. Sohn, C.R. Farrar, Damage diagnosis using time series analysis of vibration signals, *Smart Materials and Structures* 10 (3) (2001) 446–451.
[29] H. Sohn, C.R. Farrar, N.F. Hunter, K. Worden, Structural health monitoring using statistical pattern recognition, *Journal of Dynamic Systems Measurement and Control* 123 (2001) 706–711.

[30] P.J. Brockwell, R.A. Davis, *Time Series: Theory and Methods*, Springer, New York, 1991, pp. 113–118.
[31] R.J. Allemang, The modal assurance criterion—twenty years of use and abuse, *Journal of Sound and Vibration* 262 (3) (2003) 651–675.
[32] E. Castillo, *Extreme Value Theory in Engineering*, Academic Press, San Diego, 1988.
[33] K. Worden, D.W. Allen, H. Sohn, D.W. Stinemates, C.R. Farrar, Extreme Value Statistics for Damage Detection in Mechanical Structures. *Los Alamos National Laboratory Report* LA-13903-MS, 2002.
[34] C.E. Shannon, W. Weaver, *The Mathematical Theory of Communication*, University of Illinois Press, Chicago, 1949, pp. 75–83.
[35] T.R. Fasel, M.B. Kennel, M.D. Todd, E.H. Clayton, G. Park, Damage state evaluation of experimental and simulated bolted joints using ultrasonic chaotic waves, *Journal of Smart Structures and Systems* 5 (4) (2009) 329–344.
[36] T.R. Fasel, M.D. Todd, G. Park, Damage state evaluation of adhesive composite joints using chaotic ultrasonic waves, *Proceedings of the SPIE 14th Annual International Symposium on NDE for Health Monitoring and Diagnostics*, vol. 7295, San Diego, CA, March 2009, pp. 729511-1–729511-9.